Bioorganic & Medicinal Chemistry 17 (2009) 8060–8072

Contents lists available at ScienceDirect

Bioorganic & Medicinal Chemistry

journal homepage: www.elsevier.com/locate/bmc

Development and characterization of lysine based tripeptide analogues as inhibitors of Sir2 activity

Subhra Prakash Chakrabarty [a], Ramesh Ramapanicker [b,†], Roli Mishra [b], Srinivasan Chandrasekaran [b], Hemalatha Balaram [a,*]

[a] Molecular Biology and Genetics Unit, Jawaharlal Nehru Centre for Advanced Scientific Research, Jakkur, Bangalore 560064, India
[b] Department of Organic Chemistry, Indian Institute of Science, Bangalore 560012, India

ARTICLE INFO

Article history:
Received 1 August 2009
Revised 1 October 2009
Accepted 2 October 2009
Available online 9 October 2009

Keywords:
Sir2 activity
Peptide inhibitors
Carbohydrate conjugates
Click chemistry
Parabolic inhibition

ABSTRACT

Sirtuins are NAD^+ dependent deacetylases that modulate various essential cellular functions. Development of peptide based inhibitors of Sir2s would prove useful both as pharmaceutical agents and as effectors by which downstream cellular alterations can be monitored. Click chemistry that utilizes Huisgen's 1,3-dipolar cycloaddition permits attachment of novel modifications onto the side chain of lysine. Herein, we report the synthesis of peptide analogues prepared using click reactions on *N*ε-propargyloxycarbonyl protected lysine residues and their characterization as inhibitors of *Plasmodium falciparum* Sir2 activity. The peptide based inhibitors exhibited parabolic competitive inhibition with respect to acetylated-peptide substrate and parabolic non-competitive inhibition with NAD^+ supporting the formation of EI_2 and $E{\cdot}NAD^+{\cdot}I_2$ complexes. Cross-competition inhibition analysis with the non-competitive inhibitor nicotinamide (NAM) ruled out the possibility of the NAM-binding site being the second inhibitor binding site, suggesting the presence of a unique alternate pocket accommodating the inhibitor. One of these compounds was also found to be a potent inhibitor of the intraerythrocytic growth of *P. falciparum* with 50% inhibitory concentration in the micromolar range.

1. Introduction

Deacetylases are modulators of the functions of different histone and non-histone proteins. The activities of these enzymes affect the conformational state and thereby, functions of various substrate proteins. There are three classes of deacetylases with Class I and II being Zn^{2+} dependent. Class III deacetylases referred to as sirtuins (Sir2-like protein), catalyze a NAD^+ dependent reaction that results in the formation of nicotinamide, deacetylated substrate and *O*-acetyl ADP ribose (Scheme 1). *SIR2*, was the first sirtuin gene discovered from *S. cerevisiae*.[1] Subsequently, four additional genes, Hst1–4, were identified in *S. cerevisiae* with high homology to the *SIR2* gene.[2] Although some prokaryotes lack Sir2 like proteins, numerous Sir2 homologues have been discovered in many organisms ranging from bacteria to mammals, demonstrating that Sir2 is a highly conserved member of a large family of sirtuin genes.[3,4] As in yeast, most organisms have multiple homologues of sirtuins with different functions ascribed to them. Apart from being deacetylases, sirtuins from bacteria, yeast, and mammals also act as mono-ADP ribosyltransferases.[4]

Sirtuins have been implicated in various cellular processes such as life span extension, gene silencing, DNA repair, apoptosis, and different metabolic pathways, including adipogenesis, gluconeogenesis, and glucose homeostasis.[5–7] In addition, sirtuins are involved in regulation of several stress response factors, such as p53 tumor suppressor protein,[8] fork-head transcription factor,[9] and NF-kB.[10] Several important questions pertaining to the different functions of sirtuin homologues remain to be answered and the availability of different compounds that activate or repress sirtuins may prove useful in this regard. A limited number of natural and synthetic inhibitors of Sir2s are known, with the first reported synthetic inhibitor being sirtinol.[11] This was followed by the discovery of splitomicin, which was found to be an inhibitor of yeast Sir2[12] but not of human sirtuin subtypes. Recently, various analogues of splitomicin have been found to inhibit human SIRT2.[13] Further, the Sir2 inhibitor cambinol identified from a random screen is the first inhibitor which has been tried on an animal model to demonstrate its anti-cancer property.[14] One of the known synthetic sirtuin inhibitors, bis(indoyl)maleimide derivative (**12j**), competes for the NAD^+ binding pocket and inhibits the activity of human SIRT2.[15] Two natural products gluttiferone G and hyperforin, isolated from *Garcinia cochinchinensis* and *Hypericum perforatum* (St. John's wort), respectively, yielded high potency and modest selectivity for SIRT1 over SIRT2. Aristoforin, a synthetic derivative of hyperforin, exhibited similar potency and selectivity for SIRT1.[16]

* Corresponding author. Fax: +91 80 22082766.
E-mail address: hb@jncasr.ac.in (H. Balaram).
† Present address: Department of Biochemistry and Organic Chemistry, Uppsala University, Uppsala 75123, Sweden.

0968-0896/$ - see front matter © 2009 Elsevier Ltd. All rights reserved.
doi:10.1016/j.bmc.2009.10.003

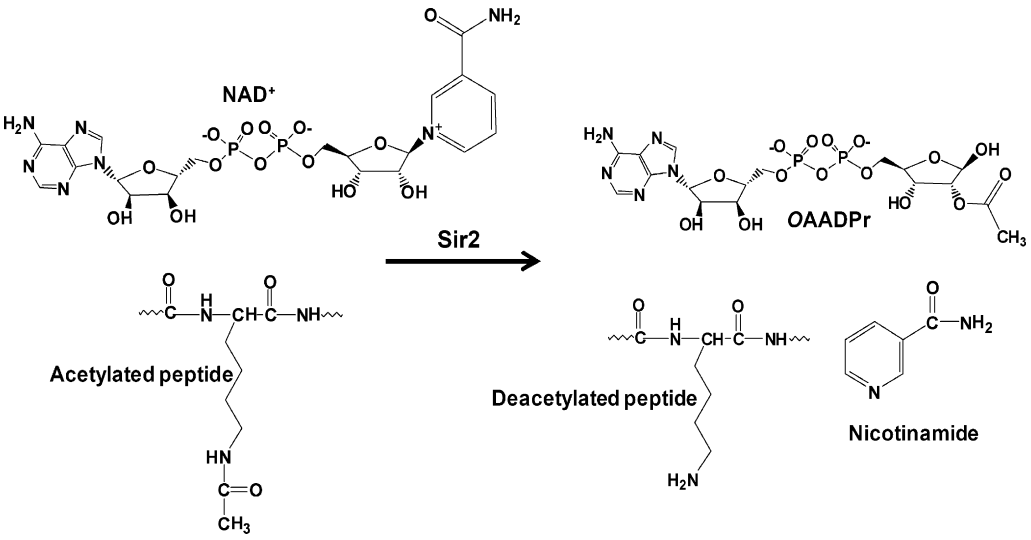

Scheme 1. Schematic representation of the protein deacetylation reaction catalyzed by Sir2.

We have earlier reported on the inhibition of *Plasmodium falciparum* Sir2 (PfSir2) by surfactin, a depsipeptide isolated from *Bacillus licheniformis* BC98.[17]

Sir2 catalyzed reaction follows a sequential kinetic mechanism where acetylated peptide binds first followed by the binding of NAD^+ leading to the formation of a ternary Michaelis–Menten complex.[18] The design of inhibitors for a bi-substrate reaction is often aided by the understanding of the catalytic mechanism. A thioacetyl lysine peptide derived from the C-terminal sequence of p53 is a competitive inhibitor with respect to the acetylated-peptide substrate and forms a non-reactive ternary complex with enzyme and NAD^+.[19] To avoid cross reaction with other NAD^+ binding enzymes development of selective sirtuin inhibitors would require preferential targeting of the acetylated peptide binding site. In a recent report, the enol form of *N*-(5-benzyloxycarbonylamino-5-phenylcarbamoylpentyl)malonamic acid ethyl ester (**2k**) has been shown to inhibit the activity of human SIRT1 potently and selectively over SIRT2 and SIRT3 by forming 2k–ADP-ribose conjugate.[20] The affinity of Sir2 inhibitors can be increased by the design of molecules that are covalently-linked analogues of both acetylated peptide and NAD^+. Suramin, a selective inhibitor of SIRT5, is an example of an inhibitor that blocks the active site of the enzyme through simultaneous binding to both NAD^+ and acetylated peptide binding sites.[21] However, suramin has also been found to inhibit several other non-Sir2 proteins due to its chemically multifunctional nature.

One of the strategies for the synthesis of peptides containing novel modifications on the lysine side chain has been through the use of click chemistry which involves Huisgen's versatile 1,3-dipolar cycloaddition reaction. (*E*)-3-(1-Cinnamyl-1*H*-1,2,3-triazol-4-yl)-*N*-ydroxyacrylamide (NSC746457), synthesized through click chemistry was found to inhibit histone deacetylases 1 (HDAC1) with an IC_{50} value of 104 ± 30 nM.[22] In attempts to generate isozyme-specific HDAC inhibitors by exploiting the variability in HDAC surface surrounding the active site, a set of triazolylphenyl-based HDAC inhibitors were constructed. Octanedioic acid{4-[1-(4-fluorobenzyl)-1*H*-[1,2,3]triazol-4-yl]phenyl}amide hydroxyamide was identified to be a selective inhibitor of HDAC6 over HDAC1 by 51-fold and a potent inhibitor with an IC_{50} value of 1.9 nM.[23]

In this paper we report on the development and kinetic characterization of peptide analogues containing novel sugar and nucleoside modifications as inhibitors of Sir2 activity. A copper(I)-catalyzed variant of the classical Huisgen reaction between a terminal alkyne and an azide, which furnishes a 1,4-substituted triazole derivative has proven to be a powerful tool for the synthesis of conjugates. We have exploited the use of propargyloxycarbonyl (Poc)[24–26] modification on the ε-amino group of lysine as an alkyne source for click reactions under the conditions reported by Sharpless[27] ($CuSO_4{\cdot}5H_2O$, sodium ascorbate, H_2O–*t*BuOH) to prepare various peptide conjugates.[28] The potency of these molecules was evaluated on the activity of recombinant *P. falciparum* Sir2. The parabolic nature of the secondary plots generated from the primary Lineweaver–Burk (LB) curves support the formation of EI_2 and $E{\cdot}NAD^+{\cdot}I_2$ complexes indicating the presence of an additional inhibitor binding site apart from the peptide binding site. Multi-inhibition studies rule out a competition between the NAM binding, D-site and the second inhibitor binding site, suggesting the presence of a unique second pocket accommodating the inhibitor.

2. Results and discussion

2.1. Synthesis of lysine conjugates using click chemistry

The strategy used for the synthesis of various conjugates (**9**–**13**), examined for the inhibition of Sir2, are detailed in Schemes 2–4. The peptides containing a lysine residue protected at the ε-amino group as a propargyloxycarbonyl (alkyne) derivative were selectively functionalized with azide derivatives of sugars/thymidine, using Cu(I) catalyzed click reactions. The peptide derivatives required for the conjugation reactions were prepared using standard solution phase peptide synthesis protocols. A selectively protected derivative of lysine, Boc-Lys(Poc)-OH (**1**) was condensed with valine methyl ester to get the dipeptide, Boc-Lys(Poc)-Val-OMe (**3**) in very good yield. The dipeptide, **3** was treated with 50% TFA to remove the Boc group and the trifluoroacetate salt (**3a**), thus obtained was treated with Boc-Phe-OH to get the tripeptide Boc-Phe-Lys(Poc)-Val-OMe (**4**) in 82% yield (Scheme 2). A benzyl ester derivative (**2**) of *N*ε-Poc lysine was prepared by treating **1** with benzyl chloride (Scheme 2). Standard procedures were used for the synthesis of the azido derivatives, **5**–**8** of galactose, D-methyl glucopyranoside, thymidine, and mannose, respectively, from the corresponding halide or tosyl derivatives using NaN_3 in DMF (Scheme 3).[29–31] Cu(I) catalyzed click reactions were performed on the Poc derivatives **2** and **4** with the azide derivatives, **5**–**8** to get the conjugates

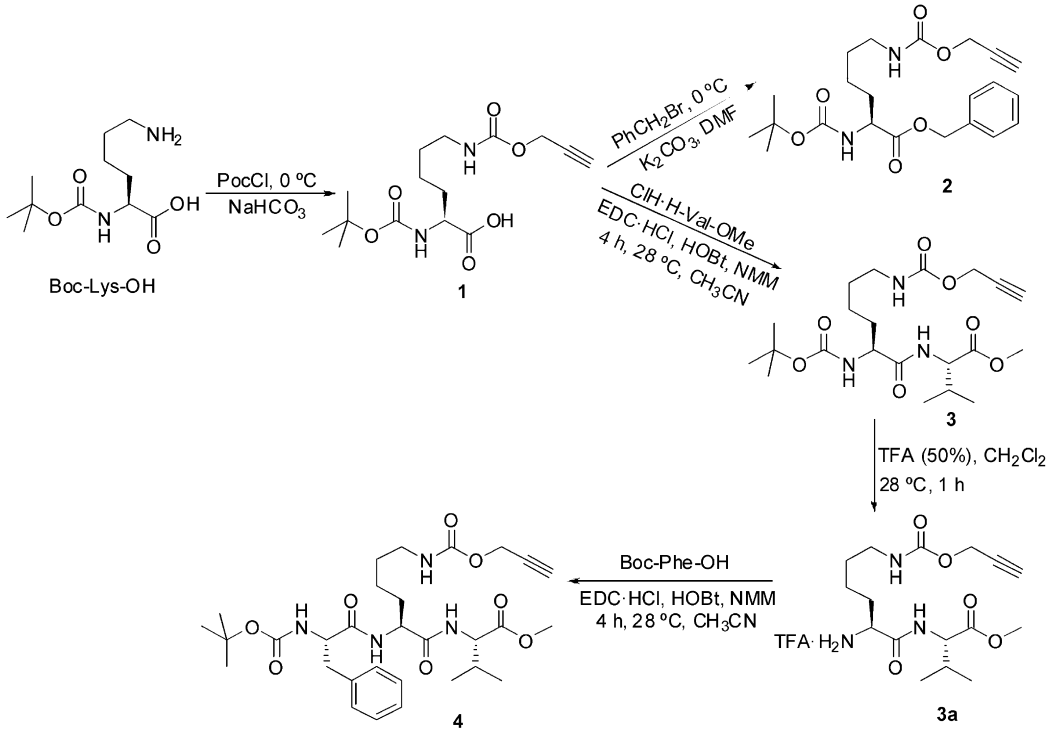

Scheme 2. Synthesis of Boc-Lys(Poc)-OBn and tripeptide from Boc-Lys(Poc)–OH.

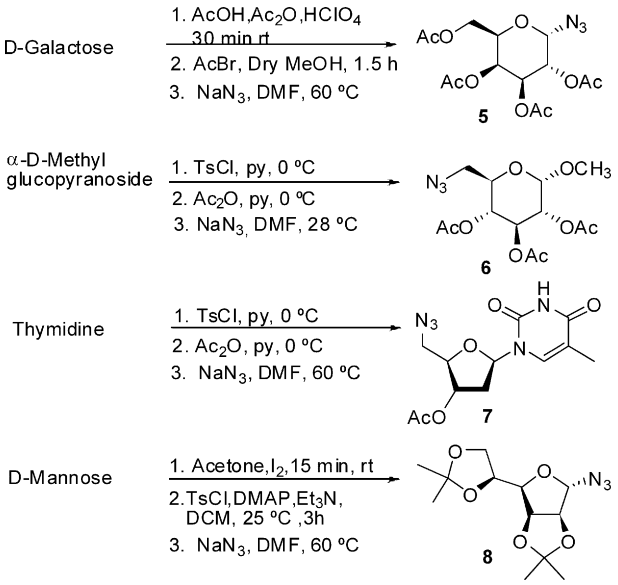

Scheme 3. Synthesis of azides from the corresponding halides.

9–**13**, with the lysine side chains modified with sugars/thymidine (Scheme 4). The click reactions yielding the 1,4-disubstituted triazole derivatives (**9**–**13**) proceeded well and the products could be isolated in high yields and purity. All the products were purified by column chromatography and were characterized spectroscopically. Purity of the compounds used for the enzyme assays were confirmed by reverse phase analytical HPLC.

The facile nature of these reactions suggests that the Poc group functions well dually as a protection for the side chain amino group of lysine during peptide synthesis and its alkyne functionality facilitates click reactions for the preparation of peptide conjugates. The high stability of the Poc group to acids can be exploited in sequential peptide synthesis. Placing the *Nε*-Poc lysine residue at suitable positions in the sequence offers an efficient entry to the synthesis of designed polypeptides, which can be functionalized using click chemistry approaches.

2.2. Synthetic peptide analogues inhibit PfSir2 deacetylase activity

The synthetic peptide analogues were examined for their ability to inhibit recombinant PfSir2 activity. The assays were carried out using 3 μM recombinant PfSir2 protein purified from an *E. coli* expression system. The IC_{50} values for **10**–**13** were 151 ± 16, 23 ± 2, 33 ± 2, and 34 ± 2 μM, respectively. The intermediate compounds **1** and **3** that are fragments of the parent molecules, and **9**, a lysine–thymidine conjugate were also examined for their ability to inhibit PfSir2 activity. Even at a concentration of 500 μM, these intermediates failed to inhibit PfSir2 activity suggesting the need for the tripeptide as the minimum inhibitory unit. The compounds **10**–**13** also inhibited human SIRT1 (CycLex, MBL International, Woburn, MA) (Fig. 1) indicating that the inhibition is a common feature across the two Sir2 homologues.

2.3. Mechanism of inhibition

The kinetic mechanism of inhibition of PfSir2 activity by **10**–**13** was examined. Double reciprocal plots of $1/v$ versus 1/[peptide] and $1/v$ versus 1/[NAD^+] at different fixed concentrations of the inhibitors, **10** (Fig. 2A and B), **11** (Fig. 3A and B), **12** (Fig. 4A and B) and **13** (Fig. 5A and B) yielded competitive and non-competitive inhibition patterns, respectively. This indicates that though the inhibitors contain sugar or nucleoside modifications they do not compete for NAD^+ binding site. The secondary plots for **10** were linear (Fig. 2C–E) while the secondary plots of the slopes (Figs. 3C, 4C, and 5C) and of slopes and intercepts (Figs. 3D–E,

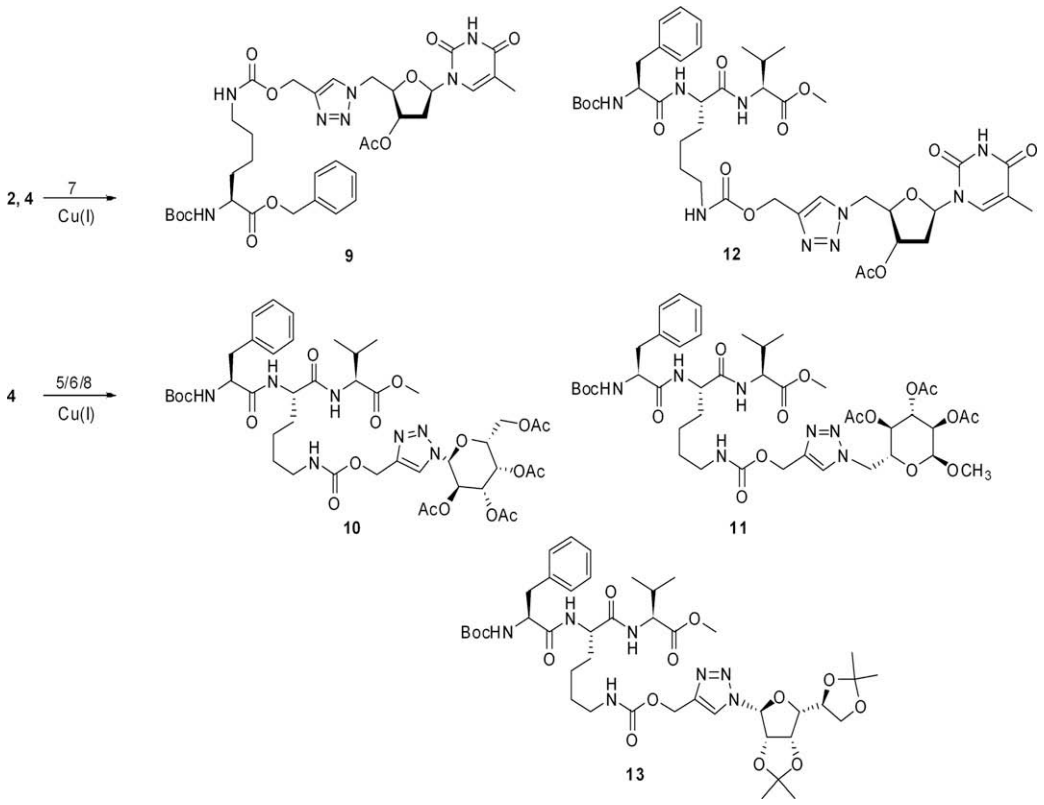

Scheme 4. Synthetic strategies for the preparation of peptide analogues and lysine thymidine analogue.

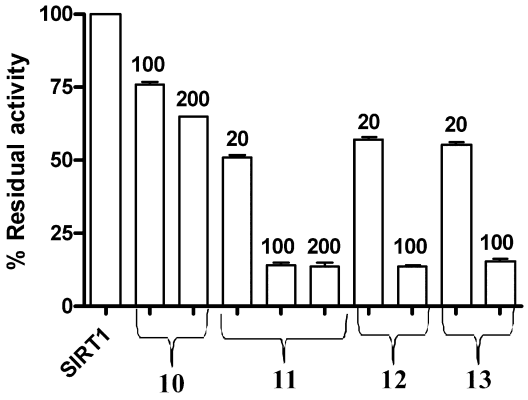

Figure 1. Inhibitory effect of **10**–**13** on human SIRT1 activity. Each bar indicates percent residual activity and numbers above bars indicate concentrations of the inhibitor in μM.

4D–E, and 5D–E) were all parabolic for **11**–**13**. Parabolic secondary plots in inhibition kinetics indicate the presence of more than one binding site for the inhibitor.[32] Also, the parabolic nature of the Dixon plots of $1/v$ versus [inhibitor (I)] for **11**–**13** provided further evidence for the presence of more than one binding site on the enzyme. The data indicate that apart from the peptide binding site, **11**–**13** have additional binding site/s on PfSir2.

The number of binding sites on the enzyme for **11**–**13** was estimated by generating plots of $1/K_i^{slope}$ versus [I] where the values of K_i^{slope} are direct slope values of lines in double reciprocal plots of $1/v$ versus 1/[peptide] or 1/[NAD^+] at fixed saturating concentration of the second substrate and fixed varying concentrations of the inhibitor. It should be noted that K_i^{slope} is not the K_i for the dissociation of an EI complex, but rather a more complex function of K_i which varies with [I].[32] Linear regression analyses using Eq. 1 were performed on the plots of $1/K_i^{slope}$ versus [I] (Fig. 6A and B) for K_i^{slope} values obtained from both the non-competitive (with respect to NAD^+) and competitive (with respect to acetylated peptide) inhibition data.

$$1/K_i^{slope} = 1/K_i^2[I] + 2/K_i \quad (1)$$

Linearity of the curves in the $1/K_i^{slope}$ versus [I] plots indicated the presence of only two binding sites for the inhibitor molecules on PfSir2 while presence of more than two binding sites would have yielded non-linear (concave-up) plots. This suggests the presence of EI_2 and $E{\cdot}NAD^+{\cdot}I_2$ complexes in the reaction mixture. At saturating substrate concentrations, no sigmoidicity was seen in v versus [I] plots, proving the absence of co-operativity in the binding of **11**–**13** to the two sites on PfSir2.

The initial velocity inhibition data for **11**–**13** fit to Eqs. 5 and 7 for single site inhibition yielded poorer statistics compared to their fits to parabolic inhibition described by Eqs. 8 and 9. Table 1 summarizes the K_i values obtained from fits of the primary plots to Eqs. 8 and 9 and, of the secondary plots to Eqs. 10 and 11. The K_i values for **11**–**13** are apparent and represent an average K_i value for binding to both the sites on the enzyme. The linearity of the secondary plots for **10** indicates a true K_i value and a single binding site on the enzyme. The K_i values for the different inhibitors with respect to peptide are largely similar, with the value for **10** being slightly higher.

To confirm the presence of EI_2 and ESI_2 (S corresponds to NAD^+) complexes with respect to the inhibitors, **11**–**13**, the initial velocity data were analyzed by constructing [S]/v versus [I] plots and fitting to Eq. 2 (Fig. 7).[33,34]

$$[S]/v = a_0 + a_1[I] + a_2[I]^2 + [S](b_0 + b_1[I] + b_2[I]^2) \quad (2)$$

where a_0, b_0, a_1, b_1, a_2, and b_2 are the coefficients depending on equilibrium constants and correspond to the presence of E, ES, EI,

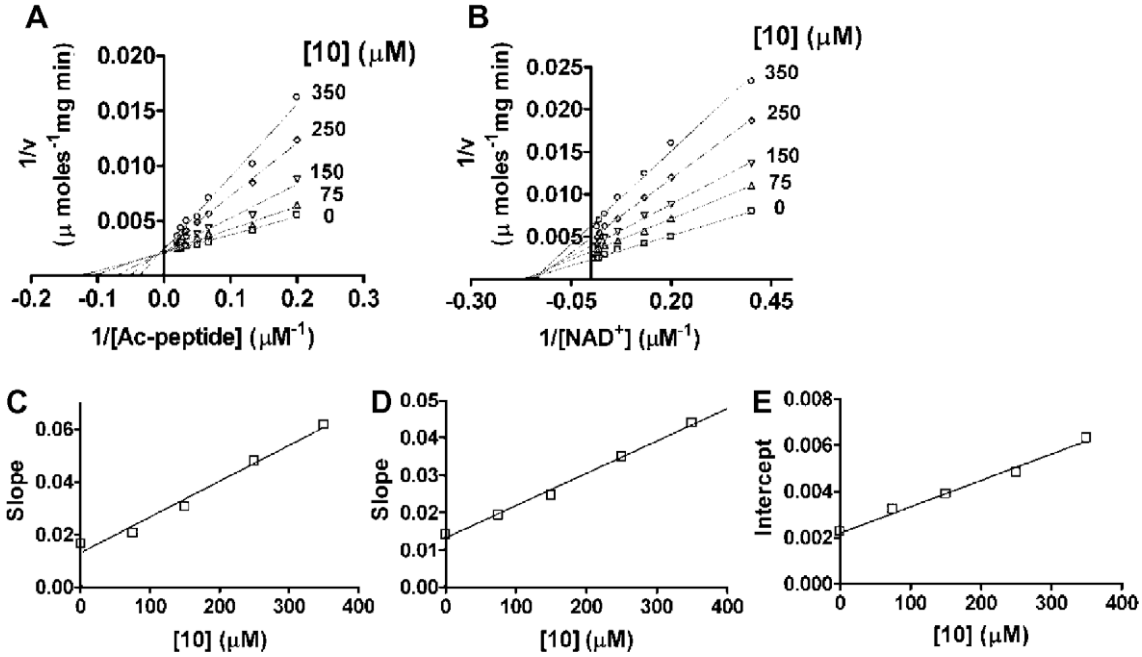

Figure 2. Lineweaver–Burk plots of PfSir2 inhibition by **10**. (A) Compound **10** exhibits competitive inhibition pattern with respect to acetylated peptide. NAD^+ concentration was 70 μM and [acetylated peptide] was varied from 1 to 50 μM. (B) Compound **10** shows non-competitive inhibition with respect to NAD^+. Acetylated peptide concentration was fixed at 30 μM while [NAD^+] was varied from 2.5 to 70 μM. The micromolar concentration of **10** is indicated against each line. (C) Secondary plot of slope versus [**10**], generated from primary plot in (A). (D) and (E), secondary plots of slope versus [**10**] and intercept versus [**10**], respectively, generated from primary plot in (B). Solid line is the curve generated from linear fit. Assays were done twice with two independently purified batches of enzyme.

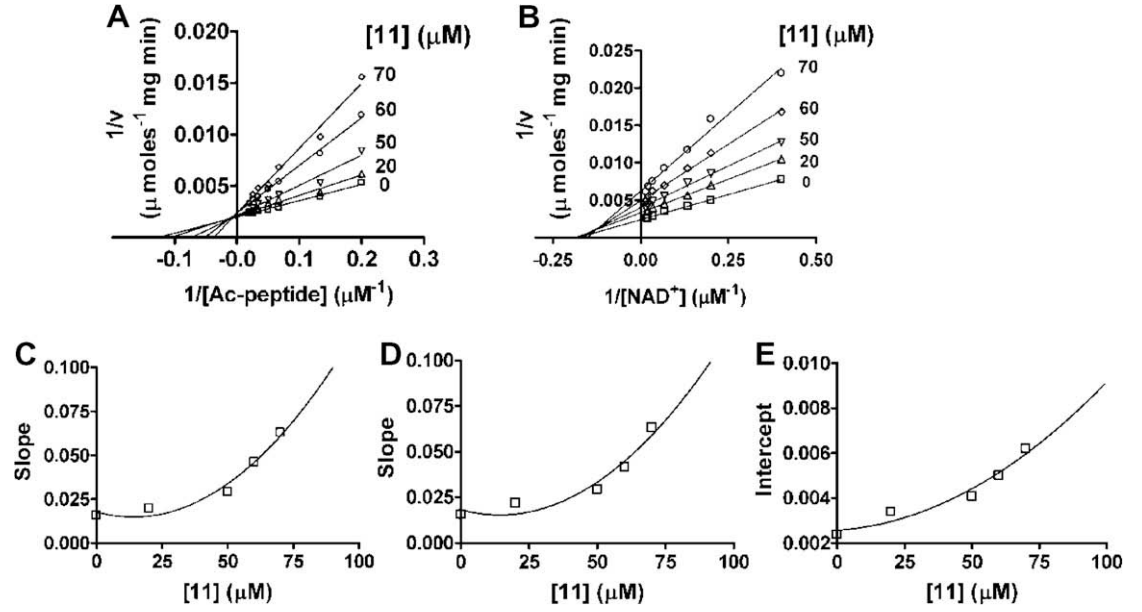

Figure 3. Lineweaver–Burk plots of PfSir2 inhibition by **11**. (A) Compound **11** shows competitive inhibition with respect to acetylated peptide. [NAD^+] was held constant at 70 μM and acetylated peptide concentration was varied from 1 to 50 μM. (B) Compound **11** exhibits non-competitive inhibition with respect to NAD^+. Acetylated peptide concentration was fixed at 30 μM while [NAD^+] was varied from 2.5 to 70 μM. The micromolar concentration of **11** is indicated against each line. (C) Secondary plot of slope versus [**11**], generated from primary plot in (A). (D) and (E), secondary plot of slope versus [**11**] and intercept versus [**11**], respectively, generated from primary plot in (B). Solid line in panels (C–E) are curves generated from polynomial second order regression analysis. Assays were done twice with two independently purified batches of enzyme.

ESI, EI_2, and ESI_2 enzyme species in the system. Non-zero values of the coefficients that are statistically significant indicate the presence of a specific complex. The three inhibitors, **11**–**13** that showed parabolic secondary plots in the LB data yielded non-zero, statistically significant values for the coefficients a_2 and b_2 for both substrates supporting the presence of EI_2 and ESI_2 complexes. Negative values were obtained for the coefficient associated with EI and ESI complexes. Compound **10** which does not show parabolic secondary plots yielded statistically significant and non-zero values for the coefficients a_2 and b_1 only. However, the value for a_2 was 100-fold lower than that obtained for **11**–**13**, indicating the low levels of EI_2 complex and higher ESI levels in the reaction mixture.

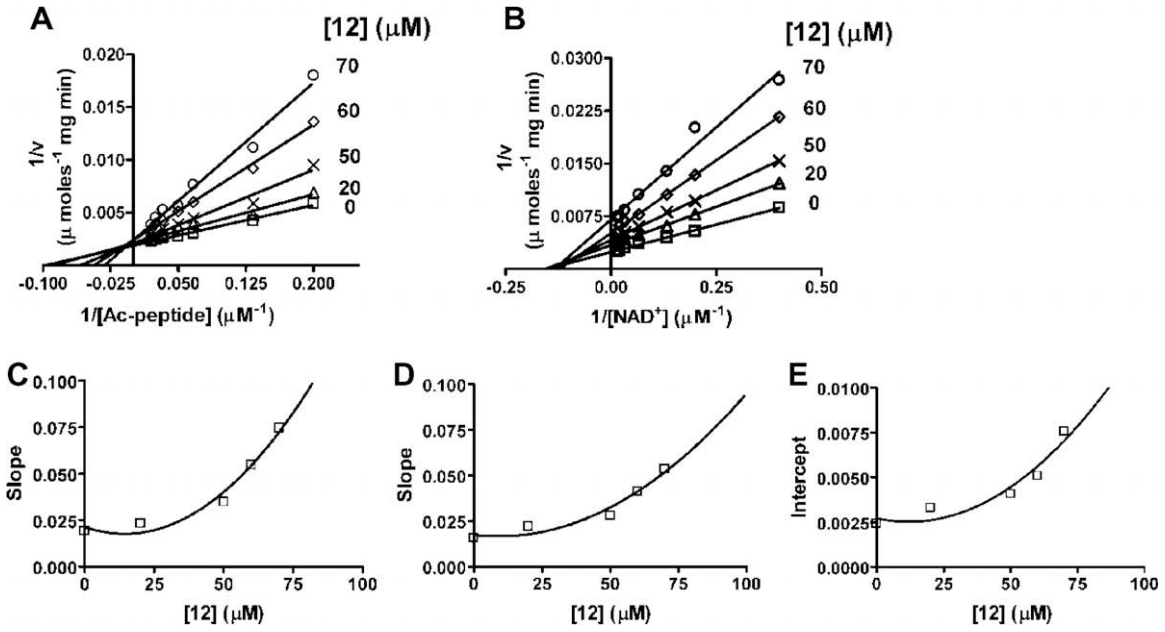

Figure 4. Lineweaver–Burk plots of PfSir2 inhibition by **12**. (A) Compound **12** shows competitive inhibition with respect to acetylated peptide. [NAD$^+$] was held constant at 70 μM and acetylated peptide concentration was varied from 1 to 50 μM. (B) Compound **12** exhibits non-competitive inhibition with respect to NAD$^+$. Acetylated peptide concentration was fixed at 30 μM while [NAD$^+$] was varied from 2.5 to 70 μM. The micromolar concentration of **12** is indicated against each line. (C) Secondary plot of slope versus [**12**], generated from primary plot in (A). (D) and (E), secondary plot of slope versus [**12**] and intercept versus [**12**], respectively, generated from primary plot in (B). Solid line in panels (C–E) are curves generated from polynomial second order regression analysis. Assays were done twice with two independently purified batches of enzyme.

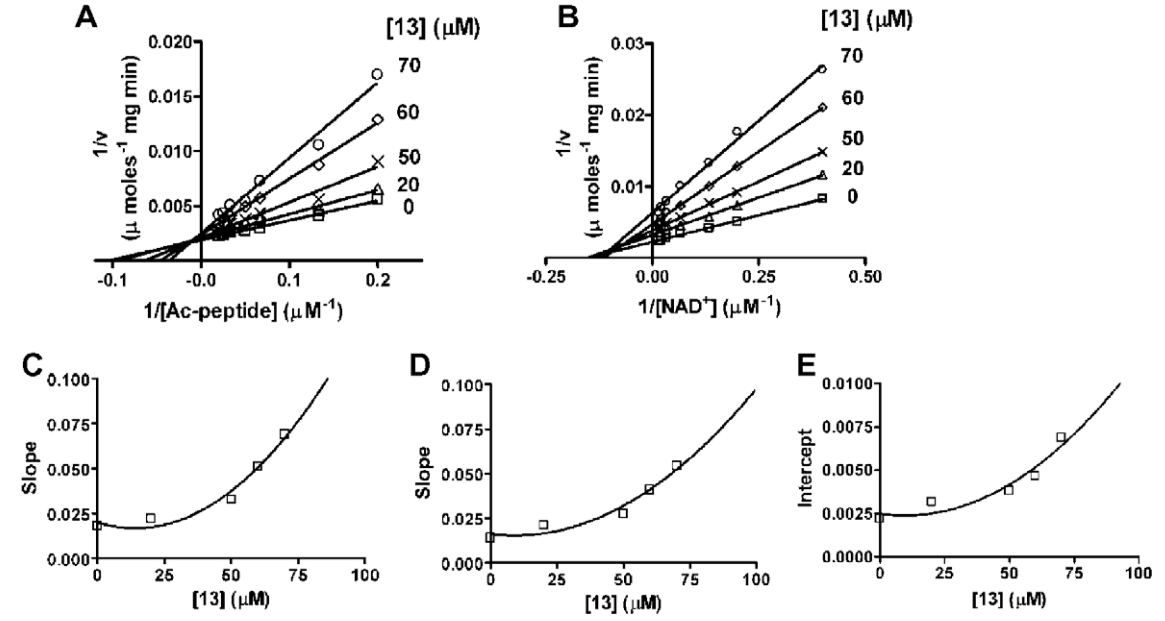

Figure 5. Lineweaver–Burk plots of PfSir2 inhibition by **13**. (A) Compound **13** shows competitive inhibition with respect to acetylated peptide. [NAD$^+$] was held constant at 70 μM and acetylated peptide concentration was varied from 1 to 50 μM. (B) Compound **13** exhibits non-competitive inhibition with respect to NAD$^+$. Acetylated peptide concentration was fixed at 30 μM while [NAD$^+$] was varied from 2.5 to 70 μM. The micromolar concentration of **13** is indicated against each line. (C) Secondary plot of slope versus [**13**], generated from primary plot in (A). (D) and (E), secondary plot of slope versus [**13**] and intercept versus [**13**], respectively, generated from primary plot in (B). Solid line in panels (C–E) are curves generated from polynomial second order regression analysis. Assays were done twice with two independently purified batches of enzyme.

2.4. Cross inhibition kinetics with NAM and 11

Inhibition kinetics presented above indicates the presence of two binding sites for **11** on PfSir2. The competitive inhibition pattern seen with respect to acetylated peptide indicates that one of the binding sites for **11** is the acetylated peptide binding site while the location of the second site is not evident from the analysis. Being a non-competitive inhibitor of NAD$^+$, compound **11** does not bind to NAD$^+$ binding site. Studies on yeast Hst2, human SIRT2, and yeast Sir2 have shown that NAM is a non-competitive inhibitor with respect to both acetylated peptide and NAD$^+$.[35] A similar NAM inhibition pattern was also seen with PfSir2.[17] From the various

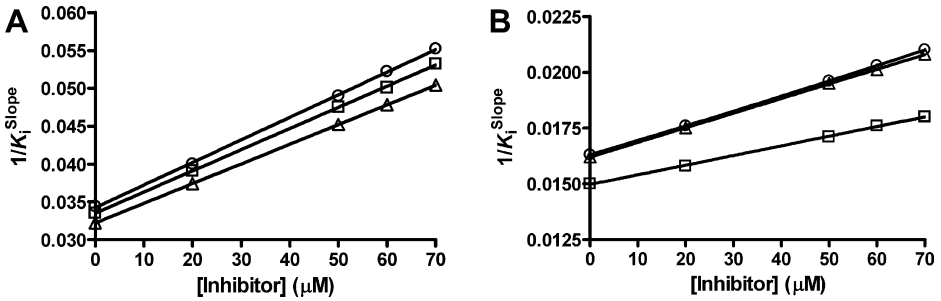

Figure 6. The plots of $1/K_i^{slope}$ versus [inhibitor **11** (□) or **12** (Δ) or **13** (○)]. Solid lines in the two panels are curves generated from linear regression analyses. K_i^{slope} values for panels (A) and (B) were derived from Lineweaver–Burk plots of competitive inhibition (with respect to peptide) in Figures 3A, 4A and 5A and non-competitive inhibition (with respect to NAD^+) in Figures 3B, 4B and 5B, respectively.

Table 1
Summary of the K_i values for compounds **10**–**13** obtained from different primary and secondary curve fits

Inhibitors	Type of inhibition	K_i from primary plot (μM)	K_i from secondary plot of slope versus [inhibitor] (μM)	K_i from secondary plot of intercept versus [inhibitor] (μM)
Compound **10** versus Ac-peptide[a]	Competitive	85 ± 11	80 ± 10	NA
Compound **10** versus NAD^+	Non-Competitive	154 ± 11	172 ± 5	193 ± 6
Compound **11** versus Ac-peptide[a]	Competitive	60 ± 7	60 ± 5	NA
Compound **11** versus NAD^+	Non-Competitive	134 ± 7	90 ± 11	119 ± 7
Compound **12** versus Ac-peptide[a]	Competitive	60 ± 7	64 ± 5	NA
Compound **12** versus NAD^+	Non-Competitive	124 ± 6	115 ± 11	113 ± 7
Compound **13** versus Ac-peptide[a]	Competitive	58 ± 7	62 ± 5	NA
Compound **13** versus NAD^+	Non-Competitive	122 ± 6	90 ± 12	125 ± 7

[a] Ac-peptide is acetylated peptide, NA—not applicable.

crystal structures of Sir2s complexed with ligands, the binding site of the NAM group of NAD^+ has been identified as C-site and found to consist of conserved residues.[36] Crystal structures of yeast Hst2 bound to an acetyl-lysine containing histone H4 peptide, adenosine 5′-diphosphate (hydroxymethyl) pyrrolidinediol (ADP-HPD), and nicotinamide (NAM) (PDB ID 2OD9) show the presence of an alternate binding site for nicotinamide.[37] This binding site referred to as the D-site has been proposed to be the structural basis for the non-competitive inhibition of NAM with respect to NAD^+. The residues that form the D pocket are largely conserved with the exception of few substitutions, implying that this binding site may be important for NAM mediated regulation of Sir2 activity. To examine the possibility of blocking NAM binding due to second site occupancy by the inhibitors **11**–**13** the cross-competition method of simultaneously investigating two inhibitors was adopted. This method can provide information on whether enzyme inhibition in the presence of two different inhibitors may be from simultaneous binding to independent sites or from mutually exclusive binding to same or overlapping sites.[32] Using this approach, the effect of binary combination of **11** and NAM was investigated. The reciprocal of initial velocity, $1/v$ was plotted against [NAM] or [**11**] to visualize the intersection pattern while the other inhibitor was kept at different fixed concentrations. The cross-competition pair formed an intersecting pattern in the second quadrant of Dixon plot when NAM was the titrant at different fixed concentrations of **11** (Fig. 8A), indicating that the binding of **11** and NAM are not mutually exclusive. For a two inhibitor system where inhibitors (I and X) are not mutually exclusive and I is linear competitive inhibitor while X is linear non-competitive inhibitor with respect to substrate, the equation describing the initial velocity is,[32]

$$1/v = K_m/V_{max}K_i[S](1 + [X]/\beta K_x)[I] + 1/V_{max}[(1 + [X]/\alpha K_x) + K_m/[S](1 + [X]/K_x)] \quad (3)$$

While for the case, where I is parabolic competitive and X is linear non-competitive inhibitor with respect to the substrate, the equation is,

$$1/v = K_m/V_{max}K_i^2[S](1 + [X]/\beta K_x)[I]^2 + 1/V_{max}[(1 + [X]/\alpha K_x) + K_m/[S](1 + [X]/K_x)] \quad (4)$$

Replots of slope and intercept from the $1/v$ versus [NAM] Dixon plot, against [**11**] would yield a straight line if the system follows Eq. 3 while the curve would be concave-up in the case of Eq. 4. We observe that both replots (Fig. 8C and D) are parabolic in nature supporting the formation of E·(**11**)$_2$·NAM complex in the system. The $1/v$ versus [**11**] Dixon plot at different fixed concentrations of NAM is parabolic in nature (Fig. 8B). This observation also supports the presence of E·(**11**)$_2$·NAM complex in the system implying the simultaneous binding of both inhibitors. The panel also shows that at higher concentration of 40 μM of NAM, the curve is linear, going to show that under this condition the PfSir2 enzyme is largely inhibited by NAM with low contribution from **11**.

Taking together these results, the kinetic scheme for inhibition of PfSir2 activity by **11** is shown in Scheme 5. The enzyme is inhibited by **11** through binding of two molecules of inhibitors resulting in the formation of both E·(**11**)$_2$ and E·(**11**)$_2$·NAD^+ dead-end complexes. The scheme also shows the presence of the complexes E·(**11**)$_2$·NAM and E·(**11**)$_2$·NAM·NAD^+. Though the binding of **11** to two sites on the PfSir2 does not exclude NAM binding, the data cannot distinguish between the complexes E·(**11**)$_2$·NAM and E·(**11**)$_2$·NAM·NAD^+.

2.5. Effect of 11 on the growth of the intraerythrocytic *P. falciparum*

We have investigated the effect of **11** on the intraerythrocytic stages of *P. falciparum* in in vitro culture (Fig. 9). The IC_{50} value for **11** is 9.8 ± 1.7 μM for the killing of intraerythrocytic stages of the parasite. Surfactin, a secondary metabolite from *B. licheniformis* that inhibits PfSir2 activity by binding to the NAD^+ site, is also an inhibitor of parasite growth in in vitro cultures.[17] NAM, a product of the Sir2 catalyzed reaction and a non-competitive inhibitor with respect to both acetylated peptide and NAD^+, when added to

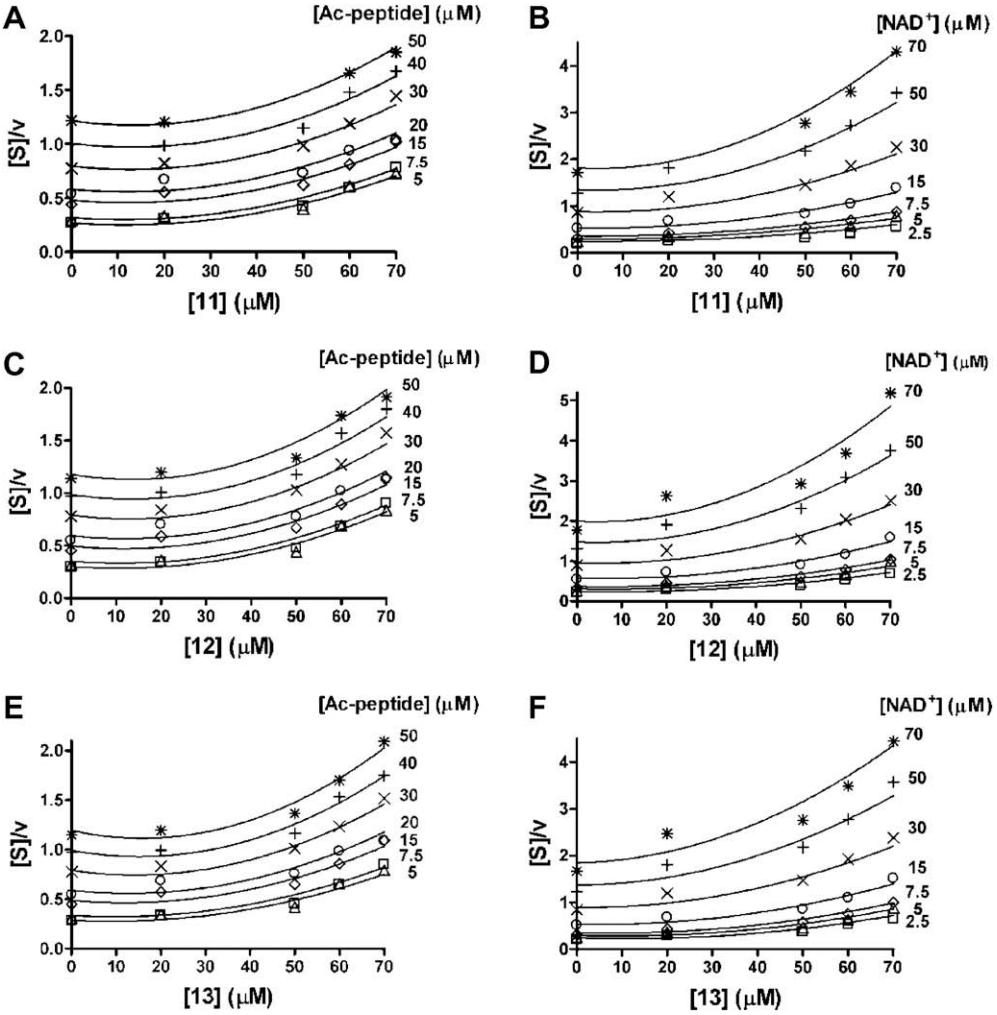

Figure 7. [S]/*v* versus [inhibitor] plots of PfSir2 inhibition by **11** (A, B), **12** (C, D) and **13** (E, F) at different fixed concentrations of peptide and NAD^+, respectively. The micromolar concentration of substrates (peptide and NAD^+) is indicated against each line. The data were fit to Eq. 2 and compared with fit to the equation ($[S]/v = a_0 + b_0[S] + a_1[I] + b_1[S][I]$) that describes a system for inhibitors having one binding site on the enzyme. For compounds **11**–**13** the preferred model is Eq. 2 and the nature of the plots is parabolic suggesting the formation of EI_2 and ESI_2 complexes in solution while a linear profile with respect to both peptide and NAD^+, would indicate the formation of EI and ESI complex.

in vitro cultures of *P. falciparum* brought about a delay in parasite growth and dispersed the localization of PfSir2 from the nucleus.[38] Hyperforin, a natural product isolated from *Hypericum perforatum* that inhibits human SIRT1 and SIRT2 activity, also exhibits antiplasmodial activity with an IC_{50} value in micromolar range.[16,39]

P. falciparum evades the host immune system by switching the expression of the erythrocyte membrane protein (EMP) surface antigens through the silencing of *var* gene expression. PfSir2 genes (PF13_0152 and PF14_0489) have been implicated to be involved in silencing of the *var* gene repertoire and also have been shown to bind to telomeric ends of chromosomes in the intraerythrocytic stages of the parasite.[40,41] Halting the process of *var* gene silencing through PfSir2 inhibition could serve to assist the process of parasite clearance by the host immune system. Knock-out of the two *P. falciparum Sir2* genes, PF13_0152 and PF14_0489, has shown that absence of either one of them is not lethal to the parasite and also established their functional redundancy in the parasite.[41] However, the effect of a simultaneous knock-out of both PfSir2 genes has not been examined. The lethality that we see with **11** could arise from simultaneous inhibition of both PfSir2 proteins suggesting that apart from modulation of *var* gene expression, the Sir2 proteins in the parasite may have other essential roles. This, however, needs further experimental validation.

3. Conclusions

Sirtuins have been implicated in numerous biological processes and availability of specific and potent inhibitors should prove to be of enormous clinical value apart from their use as tools to probe function and modulation of this important class of deacetylases. Earlier studies on inhibitors of Sir2s have mainly focused on molecules obtained from screens and hence, are largely unrelated to the structures of the two substrates. Reports on the use of peptide analogues and NAD^+ analogues have indicated that these are independently potent inhibitors of the enzyme. Our studies, for the first time, show that the tripeptides containing lysine modified via a 1,4 triazole linker with sugars/thymidine derivatives are a novel class of compounds inhibiting *P. falciparum* Sir2 activity through competition for the peptide binding pocket. Also, the observed inhibition of human SIRT1 by the peptide conjugates, along with the high degree of sequence and structure conservation in the core domain of Sir2s, suggest that these molecules may have the potential to inhibit this enzyme from other organisms. This further agrees with the fact that catalytic mechanism of different Sir2s is conserved. The utilization of click chemistry permits creation of covalent links between diverse building blocks. Herein, we have demonstrated the synthetic ease of click chemistry involving con-

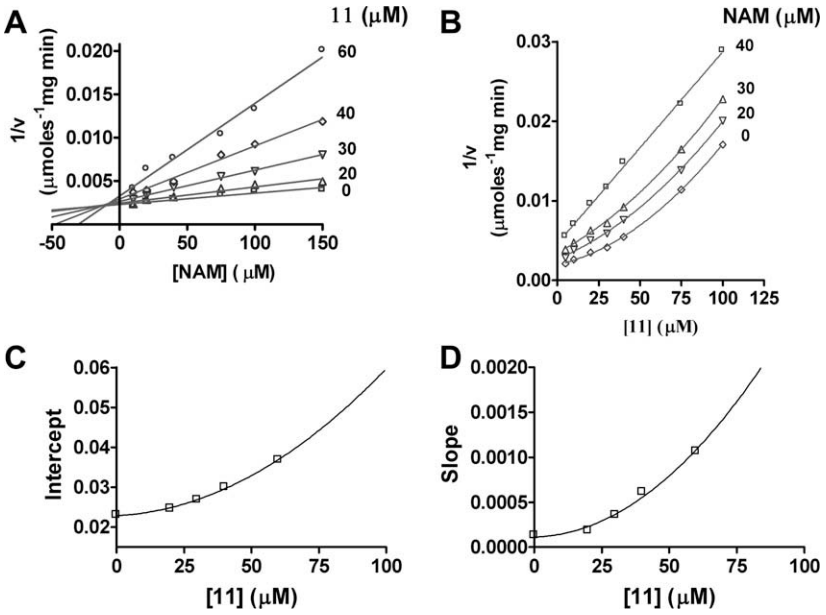

Figure 8. Cross-competition plots of PfSir2 inhibition between **11** and NAM. (A) NAM exhibits an intersecting inhibition pattern with respect to **11**. NAD^+ and acetylated peptide concentrations were held constant at 70 and 30 μM, respectively. (B) Compound **11** shows parabolic inhibition pattern with respect to NAM. The curve is linear at a NAM concentration of 40 μM. The micromolar concentrations of **11** and NAM are indicated against each line. (C) and (D), Slope and intercept obtained from reciprocal plot of (A) versus [**11**], yielded a parabola, indicating the formation of E·(**11**)$_2$·NAM complex.

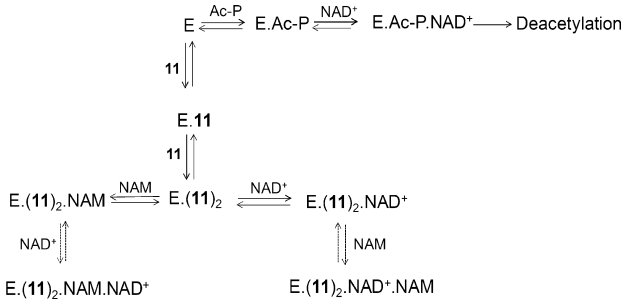

Scheme 5. Kinetic scheme for inhibition of PfSir2 activity by **11**. Ac-P is the acetylated peptide substrate.

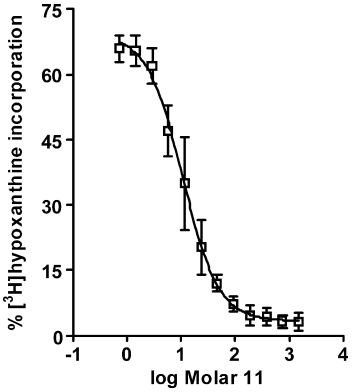

Figure 9. Effect of **11** on uptake of [^{3}H] hypoxanthine by parasitized erythrocytes in culture. Culture was treated with **11** for 24 h, followed by the addition of 1 μCi [^{3}H] hypoxanthine to each well. The cells were harvested after another 12 h and [^{3}H] hypoxanthine was quantified by scintillation counting.

densation of propargyloxycarbonyl functionalized lysine with azido derivatives of sugars/nucleosides that has resulted in excellent yields of products with high purity. The synthetic strategy described here opens up the possibility of developing a novel class of inhibitors specific to sirtuins.

4. Experimental

4.1. Materials

All bacterial growth media components were purchased from HiMedia Laboratories (Mumbai, India). Substrates used for enzyme assays and buffer components were purchased from Sigma Chemical Company (St. Louis, MO, USA). All reagents were of analytical grade and obtained from Aldrich (Steinheim, Germany). TLC was performed on commercial plates coated with Silica Gel GF254 (0.25 mm). Silica gel (230–400 mesh) was used for column chromatography. Melting points determined are uncorrected. Yields refer to chromatographically and spectroscopically pure compounds. NMR spectra were recorded on 300 or 400 MHz instruments. The following abbreviations explain the multiplicity in the spectra s = singlet, d = doublet, t = triplet, q = quartet, m = multiplet, br = broad. Coupling constants are reported wherever necessary in hertz (Hz). IR spectra were recorded on a FTIR spectrometer. The frequencies are reported in wave number (cm^{-1}) and intensities of the peaks are denoted as s (strong), w (weak), m (medium) and br (broad). High-resolution mass spectra (HRMS) were recorded on a Micromass Q-TOF mass spectrometer.

4.2. Preparation of propargyloxycarbonyl chloride (PocCl)

To a stirred solution of triphosgene (2.23 g, 7.5 mmol) in anhydrous diethyl ether (30 mL), activated charcoal (0.05 g) was added and stirred for 1 h at room temperature (28 °C). The solution was cooled to 0 °C and propargyl alcohol (0.9 mL, 15 mmol) in anhydrous diethyl ether (10 mL) was added dropwise. The resultant solution was stirred for 12 h and filtered. The diethyl ether layer was concentrated under reduced pressure (100 mm) and the remaining pale green liquid was used for reactions without any further purification. Boiling point: 118–122 °C; density (28 °C): 1.215 g/cm^3; FTIR (neat): 3303, 2982, 2131, 1777; δ_H (300 MHz,

$CDCl_3$): 2.6 (t, J = 2.4 Hz, 1H), 4.7 (d, J = 2.4 Hz, 2H); δ_C (75 MHz, $CDCl_3$): 150.2, 77.6, 74.9, 58.3.

4.3. Synthesis of Boc-Lys(Poc)-OH (1)

Commercially available Boc-Lys-OH (1.25 g, 5 mmol) was dissolved in a solution of $NaHCO_3$ (1 N, 20 mL) and NaOH (4 N, 1 mL). The solution was cooled to 0 °C, PocCl (0.55 mL, 5.5 mmol) was added dropwise and the reaction mixture was stirred for 1 h. It was allowed to come to room temperature and was stirred for additional 3 h. The reaction mixture was acidified to pH 2–3 by the slow addition of 1 N $KHSO_4$ and was extracted with ethyl acetate (3 × 25 mL). The organic layers were combined and washed with saturated citric acid solution, water and then with brine. The solvent was removed and the crude product was purified by silica gel (100–200 mesh) column chromatography and eluted with 50–70% ethyl acetate in petroleum ether to get the desired compound as colorless oil. Yield: 92%; FTIR (Neat): 3300 (br), 2128 (w), 1717 (s), 1709 (s), 1702 (s), 1692 (s); δ_H (3 00 MHz, $CDCl_3$): 6.21 (br s, 1H), 5.35 (br d, J = 7.2 Hz, 1H), 5.20 (br s, 1H), 4.68 (d, J = 1.8 Hz, 2H), 4.29 (br s, 1H), 3.16–3.21 (m, 2H), 2.49 (s, 1H), 1.84 (br s, 1H), 1.66–1.74 (m, 1H), 1.43–1.58 (m, 13H); δ_C (75 MHz, $CDCl_3$): 176.1, 156.8, 155.7, 80.1, 78.2, 74.6, 53.1, 52.4, 40.6, 31.8, 29.1, 28.3, 22.2; *m/z* (HRMS): calcd for $C_{15}H_{24}N_2O_6$+Na: 351.1532; found: 351.1522.

4.4. Preparation of Boc-Lys(Poc)-OBn (2)

Boc-Lys(Poc)-OH (**1**) (1.64 g, 5 mmol) was dissolved in DMF (10 mL). The solution was stirred and cooled to 0 °C. K_2CO_3 (0.76 g, 5.5 mmol) was added to the cold solution and the stirring was continued for 15 min. Benzyl bromide (0.65 mL, 5.5 mmol) was added to the cold solution and stirring was continued for 1 h at 0 °C. The reaction mixture was allowed to come to room temperature and the stirring was continued for additional 2 h. DMF was removed under vacuum and the compound was extracted with CH_2Cl_2, filtered and concentrated. The crude product was purified by silica gel (100–200 mesh) column chromatography and eluted with 20–30% ethyl acetate in petroleum ether to get the Poc derivative (**2**) as colorless oil. Yield: 96%; FTIR (Neat): 3342 (br), 3307 (br), 2126 (w), 1713 (s), 1710 (s), 1706 (s), 1700 (s); δ_H (300 MHz, $CDCl_3$): 7.36 (br s, 1H), 5.10–5.19 (m, 3H), 4.91 (br s, 1H), 4.66 (d, J = 2.1 Hz, 2H), 4.29–4.36 (m, 1H), 3.10–3.15 (m, 2H), 2.47 (t, J = 2.1 Hz, 1H), 1.28–1.79 (m, 15H); δ_C (75 MHz, $CDCl_3$): 172.6, 155.5, 125.3, 128.6, 128.4, 128.3, 125.3, 79.9, 78.3, 74.5, 67.0, 53.2, 52.3, 40.6, 32.2, 29.2, 28.3, 22.2; *m/z* (HRMS): calcd for $C_{22}H_{30}N_2O_6$+Na: 441.2002; found: 441.2009.

4.5. Preparation of the dipeptide Boc-Lys(Poc)-Val-OMe (3)

A solution of Boc-Lys(Poc)-OH (**1**) (0.656 g, 2 mmol), HCl·H-Val-OCH_3 (0.334 g, 2 mmol), *N*-methyl morpholine (0.66 mL, 6 mmol) and *N*-hydroxy benzotriazole (0.270 g, 2 mmol) in CH_3CN (20 mL) was cooled to 0 °C and EDC·HCl (0.576 g, 3 mmol) was added in small portions. The reaction mixture was brought to room temperature (28 °C) and stirred for 4 h. Acetonitrile was removed under vacuum and the reaction mixture was extracted with ethyl acetate (50 mL), washed with saturated citric acid solution (30 mL), saturated Na_2CO_3 (30 mL × 2), and brine (30 mL). Ethyl acetate was removed under vacuum and the dipeptide was purified by silica gel (100–200 mesh) column chromatography eluting with a solution of ethyl acetate (30–40%) in petroleum ether. The dipeptide (**3**) was isolated as a white solid in 86% yield. Mp: 78 °C; FTIR (Neat): 3313 (br), 2126 (w), 1714 (s), 1699 (s), 1683 (s), 1667 (s); δ_H (300 MHz, $CDCl_3$): 6.73 (br s, J = 9 Hz, 1H), 5.26 (br d, J = 7.8 Hz, 1H), 5.19 (br t, J = 6.6 Hz, 1H), 4.67 (d, J = 2.4 Hz, 2H), 4.53 (dd, J_1 = 9 Hz, J_2 = 5 Hz, 1H), 4.07–4.15 (m, 1H), 3.75 (s, 3H), 3.17–3.23 (m, 2H), 2.48 (t, J = 2.4 Hz, 1H), 2.09–2.34 (m, 2H), 1.78–2.34 (m, 1H), 1.35–1.71 (m, 13H), 0.94 (d, J = 7.5 Hz, 3H), 0.91 (d, J = 6.9 Hz, 3H); δ_C (75 MHz, $CDCl_3$): 172.3, 172.1, 155.7, 155.6, 80.0, 78.3, 74.5, 57.1, 54.2, 52.3, 52.2, 40.3, 31.4, 30.9, 29.2, 28.2, 22.3, 18.9, 17.6; *m/z* (HRMS): calcd for $C_{21}H_{35}N_3O_7$+Na: 464.2373; found: 464.2367.

4.6. Preparation of the tripeptide Boc-Phe-Lys(Poc)-Val-OMe (4)

The dipeptide Boc-Lys(Poc)-Val-OMe, (**3**) (0.442 g, 1 mmol) was dissolved in CH_2Cl_2 (5 mL) and TFA (5 mL) was added. The reaction mixture was stirred at room temperature (28 °C) for 30 min. CH_2Cl_2 and TFA were removed under vacuum and the crude trifluoroacetate salt (**3a**) was used without further purification. Boc-Phe-OH (0.265 g, 1 mmol) and the trifluoroacetate salt (**3a**) were dissolved in CH_3CN (10 mL). *N*-Methyl morpholine (0.33 mL, 3 mmol) and *N*-hydroxy benzotriazole (0.135 g, 1 mmol) was added to the solution and the solution was cooled to 0 °C. EDC·HCl (0.288 g, 1.5 mmol) were added to the solution in small portions, and the reaction mixture was allowed to attain room temperature (28 °C) and, was stirred for 4 h. Acetonitrile was removed under vacuum and the reaction mixture was extracted with ethyl acetate (30 mL), washed with saturated citric acid solution (20 mL), saturated Na_2CO_3 (20 mL × 2), and brine (20 mL). Ethyl acetate was removed under vacuum and the tripeptide was purified by silica gel (100–200 mesh) column chromatography eluting with a solution of ethyl acetate (30–40%) in petroleum ether. The tripeptide (**4**) was obtained as white solid in 82% yield. Mp: 89 °C; FTIR (Neat): 3302 (br), 2126 (w), 1709 (s), 1646 (s); δ_H (300 MHz, $CDCl_3$): 7.17–7.30 (m, 5H), 6.99 (br d, J = 7.2 Hz, 1H), 6.92 (br d, J = 8.4 Hz, 1H), 5.41 (br t, J = 5 Hz, 1H), 5.26 (br d, J = 7.8 Hz, 1H), 4.66 (d, J = 2.4 Hz, 2H), 4.44–4.54 (m, 3H), 3.75 (s, 3H), 3.00–3.18 (m, 4H), 2.64 (t, J = 2.4 Hz, 1H), 1.75–1.87 (m, 1H), 1.26–1.70 (m, 15H), 0.92 (t, J = 7.5 Hz, 6H); δ_C (75 MHz, $CDCl_3$): 172.2, 171.7, 171.3, 155.6, 155.4, 136.5, 129.2, 128.4, 126.7, 80.0, 78.4, 74.4, 57.3, 55.5, 52.8, 52.2, 40.3, 38.1, 31.7, 30.7, 28.9, 28.1, 21.9, 18.9, 17.7; *m/z* (HRMS): calcd for $C_{30}H_{44}N_4O_8$+-Na: 611.3057; found: 611.3059.

4.7. Preparation of galactose derived azide (5)

The azide derivative (**5**) of galactose was prepared by previously reported procedure[29] as a colorless solid in 92% yield. Mp: 101–102 °C (lit: mp: 96 °C); δ_H (300 MHz, $CDCl_3$): 5.40 (br s, 1H), 5.15 (t, J = 10.4 Hz, 1H), 5.01 (br s, 1H), 4.58 (d, J = 8.5 Hz, 1H), 4.13–4.17 (m, 2H), 3.99 (t, J = 5.9 Hz, 1H), 2.10 (s, 3H), 2.09 (s, 3H), 2.09 (s, 3H), 2.04 (s, 3H); δ_C (75 MHz, $CDCl_3$): 170.3, 170.2, 169.8, 169.3, 88.2, 72.8, 70.7, 68.0, 66.8, 61.2, 20.7, 20.7, 20.6, 20.5. *m/z* (HRMS): calcd for $C_{14}H_{19}N_3O_9$+Na: 396.1019; found: 396.1016.

4.8. Preparation of the glucose derived azide (6)

The azide derivative (**6**) of glucose was prepared by earlier reported procedure.[30] Yield: 62% (overall); mp: 129 °C; FTIR (Neat): 2104 (s), 1749 (s); δ_H (300 MHz, $CDCl_3$): 5.40 (d, J = 3.6 Hz, 1H), 5.34 (dd, J_1 = 10.8 Hz, J_2 = 3.3 Hz, 1H), 5.16 (dd, J_1 = 11 Hz, J_2 = 3.6 Hz, 1H), 5.03 (d, J = 3.3 Hz, 1H), 4.11–4.15 (m, 1H), 3.45 (s, 3H), 3.15 (dd, J_1 = 12.9 Hz, J_2 = 3.9 Hz, 1H), 2.17 (s, 3H), 2.10 (s, 3H), 1.99 (s, 3H); δ_C (75 MHz, $CDCl_3$): 170.3, 170.1, 169.8, 97.2, 69.0, 68.0, 67.9, 67.5, 55.6, 50.8, 20.7, 20.5; *m/z* (HRMS): calcd for $C_{13}H_{19}N_3O_8$+Na: 368.1070; found: 368.1067.

4.9. Preparation of the thymidine derived azide (7)

Thymidine (0.484 g, 2 mmol) was dissolved in pyridine (5 mL) and the solution was cooled to 0 °C. Tosyl chloride (0.42 g,

2.2 mmol) was added to the cold solution with stirring. Stirring was continued for 6 h and acetic anhydride (1 mL) was added to the reaction mixture. The solution was stirred for additional 8 h and the solution was diluted with CH_2Cl_2 (30 mL). The solution of the *O*-tosyl derivative, was washed with 1 N HCl (3 × 30 mL) and then with brine (30 mL). The product was purified by silica gel (100–200 mesh) column chromatography eluting with methanol in chloroform.

The *O*-tosyl derivative of thymidine (0.438 g, 1 mmol) was dissolved in DMF (5 mL) and sodium azide (0.98 g, 1.5 mmol) was added to the solution with stirring. The reaction mixture was allowed to stir till the complete disappearance of starting material in TLC. DMF was removed under vacuum and the products were extracted with CH_2Cl_2 (25 mL). The solvent was removed under vacuum and the product was purified by silica gel (100–200 mesh) column chromatography eluting with $CHCl_3$/MeOH and the azide derivative (**7**) was isolated as a colorless liquid. Yield: 76% (overall); FTIR (Neat): 3186 (br), 2105 (s), 1737 (s), 1703 (s), 1693 (s); δ_H (300 MHz, $CDCl_3$): 9.78 (br s, 1H), 7.39 (s, 1H), 6.35 (dd, J_1 = 8.4 Hz, J_2 = 5.6 Hz, 1H), 5.20 (d, J = 6 Hz, 1H), 4.11 (d, J = 2 Hz, 1H), 3.71–3.79 (m, 2H), 2.39–2.48 (m, 1H), 2.21–2.29 (m, 1H), 2.12 (s, 3H), 1.96 (s, 3H); δ_C (75 MHz, $CDCl_3$): 170.6, 163.8, 150.6, 134.8, 111.8, 84.3, 74.5, 52.5, 36.9, 20.8, 12.6; *m/z* (HRMS): calcd for $C_{12}H_{15}N_5O_5$+Na: 332.0971; found: 332.0968.

4.10. Preparation of the mannose derived azide (8)

The azide derivative, **8** (Scheme 3) of mannose was prepared using a previously reported method.[31]

4.11. Procedure for the synthesis of the lysine–thymidine conjugate (9)

The Boc-Lys(Poc)-OBn derivative (**2**; Scheme 2) (0.5 mmol) and the azide derivative of thymidine (**7**; Scheme 3) (0.5 mmol) were dissolved in *tert*-butanol (5 mL) and H_2O (10 mL). The solution was stirred well and $CuSO_4{\cdot}5H_2O$ (2 mg, 0.005 mmol) and sodium ascorbate (5 mg, 0.025 mmol) were added. The reaction mixture was stirred at room temperature, till the complete disappearance of the starting materials in TLC. Saturated brine (20 mL) was added to the reaction mixture and the addition product was extracted with ethyl acetate (3 × 35 mL). The solution was dried over anhydrous Na_2SO_4 and concentrated. The product was purified through a column of silica gel (60–120 mesh) with ethyl acetate. White crystalline solid; mp: 63.7 °C; Yield: 90%; FTIR (Neat): 3343 (br), 1702 (s), 1698 (s); δ_H (300 MHz, $CDCl_3$): 10.07 (s, 1H), 7.75 (s, 1H), 7.35 (br s, 5H), 6.82 (s, 1H), 6.20 (br t, J = 6.0 Hz, 1H), 5.10–5.30 (m, 8H), 4.96 (br s, 1H), 4.30–4.32 (m, 2H), 4.12 (q, J = 7.5 Hz, 2H), 2.31–2.38 (m, 2H), 2.12 (s, 3H), 1.90 (s, 3H), 1.77 (br s, 1H), 1.64 (br s, 1H), 1.43 (br s, 13 H); δ_C (75 MHz, $CDCl_3$): 172.6, 170.6, 163.4, 156.1, 155.4, 150.2, 146.8, 143.6, 135.3, 128.5, 128.4, 128.2, 125.7, 111.8, 85.0, 81.8, 79.9, 74.1, 66.9, 57.7, 53.2, 51.0, 40.5, 35.9, 32.1, 29.1, 28.2, 22.2, 20.7, 12.4; *m/z* (HRMS): calcd for $C_{34}N_{45}H_7O_{11}$+Na: 750.3075; found: 750.3074.

4.12. Synthesis of the tripeptide conjugates (10–13)

The reactions between *N*-Poc lysine tripeptide derivative (**4**; Scheme 2) and the azide derivatives (**5**–**8**; Scheme 3) were performed as mentioned above.

4.12.1. Compound 10

Yield: 85%; FTIR (Neat): 3319 (br), 1747 (s), 1651 (s); δ_H (300 MHz, $CDCl_3$): 7.94 (s, 1H), 6.79–7.29 (m, 5H), 6.79–6.93 (m, 2H), 5.87 (d, J = 10 Hz, 1H), 5.55 (t, J = 9 Hz, 2H), 5.13–5.38 (m, 5H), 4.42–4.48 (m, 2H), 4.08–4.27 (m, 3H), 3.71 (s, 3H), 2.96–3.16 (m, 4H), 1.88–2.22 (m, 13H), 1.23–1.40 (m, 16H), 0.88–0.93 (m, 6H); δ_C (75 MHz, $CDCl_3$): 172.2, 171.5, 171.1, 170.2, 169.9, 169.7, 168.9, 156.2, 155.5, 144.1, 136.4, 129.2, 128.5, 126.8, 122.2, 80.2, 73.9, 70.7, 67.9, 66.8, 61.1, 60.3, 57.5, 57.3, 55.6, 52.1, 40.4, 38.0, 31.7, 30.8, 29.6, 29.0, 28.1, 22.0, 20.9, 20.5, 20.1, 18.9; *m/z* (HRMS): calcd for $C_{44}H_{63}N_7O_{17}$+Na: 984.4178; found: 984.4122.

4.12.2. Compound 11

White solid; mp: 67.8 °C; yield: 88%; FTIR (Neat): 3313 (br), 1751 (s), 1720 (s), 1655 (s), 1648 (s); δ_H (300 MHz, $CDCl_3$): 7.78 (s, 1H), 7.17–7.27 (m, 5H), 6.74 (br d, J = 6 Hz, 1H), 6.60 (br d, J = 8.1 Hz, 1H), 5.38–5.51 (m, 4H), 5.17 (s, 1H), 4.83–4.90 (m, 3H), 4.36–4.58 (m, 5H), 4.17 (t, J = 7.2 Hz, 1H), 3.7 (s, 3H), 3.11 (m, 6H), 2.95–3.00 (m, 1H), 2.15–2.18 (m, 1H), 2.09 (s, 3H), 2.06 (s, 3H), 2.01, (s, 3H), 1.75–1.80 (m, 1H), 1.60–1.64 (m, 1H), 1.46 (br s, 2H), 1.36 (s, 9H), 1.26–1.32 (m, 2H), 0.93 (d, J = 5.2 Hz, 3H), 0.91 (d, J = 5.2 Hz, 3H); δ_C (75 MHz, $CDCl_3$): 172.2, 171.6, 171.3, 170.0, 169.8, 156.2, 155.4, 143.5, 136.5, 129.2, 128.4, 126.7, 125.2, 96.4, 79.9, 70.6, 69.9, 69.6, 67.6, 57.5, 57.3, 55.3, 52.8, 52.1, 50.6, 40.3, 38.1, 31.7, 30.7, 29.0, 28.1, 22.0, 20.5, 18.9, 17.8; *m/z* (HRMS): calcd for $C_{43}H_{63}N_7O_{16}$+Na: 956.4229; found: 956.4233.

4.12.3. Compound 12

Yield: 86%; FTIR (Neat): 3788 (br), 3301 (br), 1703 (s), 1693 (s); δ_H (400 MHz, $CDCl_3$): 7.75 (s, 1H), 7.16–7.28 (m, 5H), 7.10 (m, 1H), 6.60 (br s, 1H), 6.16–6.18 (m, 1H), 5.09–5.35 (m, 5H), 4.73–4.79 (m, 2H), 4.68 (d, J = 12 Hz, 1H), 4.51 (m, 5H), 4.29 (d, J = 3 Hz, 1H), 4.11 (dd, J_1 = 6 Hz, J_2 = 9 Hz, 1H), 3.74 (s, 3H), 2.74–3.13 (m, 6H), 2.13 (s, 3H), 2.04 (s, 2H), 1.91 (s, 3H), 1.36–1.40 (m, 11H), 1.23–1.28 (m, 2H), 0.91 (t, J = 9 Hz, 6H); δ_C (100 MHz, $CDCl_3$): 172.8, 172.5, 172.8, 172.1, 171.7, 171.5, 171.1, 170.5, 156.2, 155.4, 150.2, 136.5, 135.5, 135.3, 129.3, 128.6, 128.5, 126.9, 126.8, 126.1, 111.9, 81.7, 80.4, 80.2, 80.1, 60.3, 57.8, 57.3, 52.2, 50.8, 40.4, 38.2, 35.8, 30.9, 29.0, 28.2, 22.1, 21.0, 20.7, 18.9, 17.8, 14.1, 12.4. *m/z* (HRMS): calcd for $C_{42}H_{58}N_8O_{14}$+Na: 921.3970; found: 920.4091.

4.12.4. Compound 13

Yield: 85%; FTIR (Neat): 3308 (br), 1714 (s), 1561 (s); δ_H (300 MHz, $CDCl_3$): 7.29 (s, 1H), 7.28–7.21 (m, 6H), 7.18 (br, 1H), 7.16 (br s, 1H), 6.09 (d, J = 3 Hz, 1H), 5.19 (s, 3H), 4.84–4.96 (m, 1H), 4.43–4.52 (m, 3H), 3.99–4.15 (m, 2H), 3.74 (s, 3H), 2.05–2.17 (m, 1H), 1.55 (d, J = 6 Hz, 2H), 1.46 (s, 1H), 1.44 (s, 1H), 1.39 (s, 9H), 0.93–0.86 (m, 6H); δ_C (75 MHz, $CDCl_3$): 172.2, 171.5, 171.2, 156.2, 155.4, 136.5, 129.8, 129.2, 128.5, 126.8, 113.8, 109.5, 88.8, 88.0, 79.6, 79.3, 79.1, 78.2, 76.5, 72.5, 69.5, 66.7, 60.3, 57.6, 57.4, 55.7, 52.9, 52.1, 40.4, 38.1, 31.6, 30.8, 29.6, 29.0, 28.9, 28.1, 26.9, 25.4, 25.0, 24.0, 22.0, 18.9, 17.8, 14.1; *m/z* (HRMS): calcd for $C_{42}H_{63}N_7O_{13}$+Na: 896.4382; found: 896.4380.

4.13. Purification of recombinant *P. falciparum* Sir2 (PfSir2)

PfSir2 (PF13_0152) gene was cloned into pET 28b vector and expressed in BL21 (DE3) strain of *E. coli* as a C-terminal His-tagged fusion protein. The protein was purified as reported earlier.[17] Purification involved the incubation of cell lysate with Ni-NTA beads followed by elution of bound PfSir2 with different imidazole concentrations. The fractions were checked on SDS–PAGE,[42] pooled, dialyzed against 10 mM Tris–HCl, pH 8.0, 20% glycerol, 500 mM NaCl and 2 mM DTT and, concentrated. Protein concentration was estimated by the method of Bradford using BSA as standard.[43]

4.14. Deacetylation assay

A FRET based assay was used to measure PfSir2 activity. A synthetic peptide containing an acetylated lysine group and a donor–

acceptor pair (EDANS–DABCYL) was used as substrate. Upon deacetylation by Sir2, the peptide becomes a substrate for cleavage by trypsin resulting in separation of the donor and acceptor pair and thereby, an increase in the fluorescence intensity. For activity measurements, 100 μL of a reaction mixture containing 5 mM Tris–HCl, pH 8.0, 10 μM trichostatin A, 75 ng trypsin and 3 μM PfSir2 were used. All assays were carried out at 37 °C on a Hitachi F-2500 spectrofluorimeter (Hitachi, High-Technologies Corporation, Tokyo, Japan) fitted with a water circulated cell holder. The temperature was maintained using JULABO F25 (JULABO Labortechnik GmbH, Seelbach, Germany) water bath. Unit activity was calculated by estimating total enhancement in fluorescence intensity on complete digestion of peptide by treating the substrate with Proteinase K, a non-specific protease. The purified enzyme was found to have a specific activity of 47 nmol mg^{-1} min^{-1}. To monitor the effect of **1**, **3**, and **9**–**13** on PfSir2 activity, the enzyme was preincubated with the required concentrations of the inhibitors for 5 min prior to addition to the assay mixture.

4.15. Inhibition kinetics

Inhibition patterns were determined by measuring the initial reaction velocity at varying concentration of one substrate, fixed concentration of the second substrate and different fixed concentrations of the inhibitor.[32] To obtain values for the kinetic parameters the data were analyzed by non-linear regression analysis. Lineweaver–Burk (LB) and related secondary plots were constructed for each inhibitor and variable substrate and, the pattern examined. Eqs. 5–7 describe competitive, uncompetitive, and non-competitive inhibition, respectively.

$$v = V_{max}[S]/(K_m(1 + [I]/K_i) + [S]) \quad (5)$$

$$v = V_{max}[S]/(K_m + [S](1 + [I]/K_i)) \quad (6)$$

$$v = V_{max}[S]/(K_m(1 + [I]/K_i) + [S](1 + [I]/K_i)) \quad (7)$$

where K_m is the Michaelis constant for the variable substrate, K_i is the inhibition constant, [S] is the variable substrate concentration, and [I] is the inhibitor concentration. The above equations are valid only when enzyme binds to one molecule of inhibitor. When two molecules of inhibitor are involved in the binding process with enzyme alone or with enzyme–substrate complex, the equations become second order polynomial with respect to the inhibitor.[32] Under these conditions, the equations for competitive and non-competitive inhibition are,

$$v = V_{max}[S]/(K_m(1 + [I]/K_i)^2 + [S]) \quad (8)$$

$$v = V_{max}[S]/(K_m(1 + [I]/K_i)2 + [S](1 + [I]/K_i)^2) \quad (9)$$

The slope and intercept replots for the above-mentioned cases are non-linear in nature indicating multiple binding sites. Non-linear regression analyses were performed on secondary plots by fit to Eqs. (10) and (11) using GraphPad Prism, version 4 (GraphPad Software Inc., San Diego, CA) and K_i values were determined for the different inhibitors.

$$\text{Slope} = K_m/V_{max}(1 + [I]/K_i)^2 \quad (10)$$

$$\text{Intercept} = 1/V_{max}(1 + [I]/K_i)^2 \quad (11)$$

The best fits were selected on the basis of *F* test and *P* value.

4.16. Cross-competition assay

Cross inhibition studies were performed between nicotinamide (NAM) and **11** keeping both NAD^+ and acetylated peptide concentrations saturating. Inhibition plots were generated by measuring the initial velocity with one inhibitor as titrant at different fixed concentrations of other inhibitor. Reciprocal of velocities were plotted graphically against the inhibitor concentrations and linear regression analyses were carried out using GraphPad Prism, version 4. Both NAM and **11** concentrations were varied from 5 to 150 μM and, all assays were done at 37 °C temperature.

4.17. Cytotoxicity assay

The 3D7 strain of *P. falciparum* was cultivated in vitro using the method described by Trager and Jensen.[44] Parasites were maintained in human O^+ erythrocytes isolated from blood collected from healthy volunteers, at 5% hematocrit in RPMI 1640 (Sigma Chemical Co., St. Louis, USA) containing 10% human serum. The antiplasmodial activity was measured using previously reported methods.[45] Compound **11** was dissolved in dimethyl sulfoxide (DMSO) and the compound serially diluted twofold over the concentration range 400 to 0.2 μM. Each well contained 250 μL of cell suspension at 2% parasitemia and 2% hematocrit. Parasitized and non-parasitized erythrocytes and solvent controls were incorporated in all the tests. The plates were incubated at 37 °C in a candle jar. After 24 h, each well was pulsed with 10 μL of PBS containing 1.0 μCi of [^{3}H] hypoxanthine, and the plates incubated for another 12 h. The contents of each well were then harvested onto glass fiber filters using a Combi-12 automated cell harvester (Molecular Devices, Sunnyvale, CA), washed extensively with distilled water and dried. The radioactivity incorporated in the nucleotide pool was measured as disintegrations per minute using a Wallac 1409 (Wallac Oy, Turku, Finland) liquid scintillation counter. The experiment was done twice in duplicate. For test samples the percent radioactivity incorporated with respect to the control was plotted against the logarithm of the drug concentration. The concentration causing 50% inhibition of radioisotope incorporation (IC_{50}) was determined by interpolation. A parallel experiment by microscopy, using Giemsa-stained smears, was also conducted.

Acknowledgements

This project was supported by grants from Council of Scientific and Industrial Research (CSIR) and CSIR-NMITLI, Govt. of India. We thank Y. K. Saikumari for providing us with the synthetic peptide substrate. We acknowledge M. P. Bopanna for parasite assay and Anubhab Roy (Engineering Mechanics Unit, JNCASR) for the generous help and clarifications on equations used for curve fitting. We thank Bharath Srinivasan for the extensive time spent on discussion.

References and notes

1. Shore, D.; Squire, M.; Nasmyth, K. A. *EMBO J.* **1984**, *3*, 2817.
2. Rine, J.; Herskowitz, I. *Genetics* **1987**, *116*, 9.
3. Frye, R. A. *Biochem. Biophys. Res. Commun.* **2000**, *273*, 793.
4. Michan, S.; Sinclair, D. *Biochem. J.* **2007**, *404*, 1.
5. Kaeberlein, M.; McVey, M.; Guarente, L. *Genes. Dev.* **1999**, *13*, 2570.
6. Rogina, B.; Helfand, S. L. *Proc. Natl. Acad. Sci. U.S.A.* **2004**, *101*, 15998.
7. Bordone, L.; Motta, M. C.; Picard, F.; Robinson, A.; Jhala, U. S.; Apfeld, J.; McDonagh, T.; Lemieux, M.; McBurney, M.; Szilvasi, A.; Easlon, E. J.; Lin, S. J.; Guarente, L. *PLoS. Biol.* **2006**, *4*, e31.
8. Langley, E.; Pearson, M.; Faretta, M.; Bauer, U. M.; Frye, R. A.; Minucci, S.; Pelicci, P. G.; Kouzarides, T. *EMBO J.* **2002**, *21*, 2383.
9. Motta, M. C.; Divecha, N.; Lemieux, M.; Kamel, C.; Chen, D.; Gu, W.; Bultsma, Y.; McBurney, M.; Guarente, L. *Cell* **2004**, *116*, 551.
10. Yeung, F.; Hoberg, J. E.; Ramsey, C. S.; Keller, M. D.; Jones, D. R.; Frye, R. A.; Mayo, M. W. *EMBO J.* **2004**, *23*, 2369.
11. Grozinger, C. M.; Chao, E. D.; Blackwell, H. E.; Moazed, D.; Schreiber, S. L. *J. Biol. Chem.* **2001**, *276*, 38837.
12. Bedalov, A.; Gatbonton, T.; Irvine, W. P.; Gottschling, D. E.; Simon, J. A. *Proc. Natl. Acad. Sci. U.S.A.* **2001**, *98*, 15113.
13. Neugebauer, R. C.; Uchiechowska, U.; Meier, R.; Hruby, H.; Valkov, V.; Verdin, E.; Sippl, W.; Jung, M. *J. Med. Chem.* **2008**, *51*, 1203.
14. Heltweg, B.; Gatbonton, T.; Schuler, A. D.; Posakony, J.; Li, H.; Goehle, S.; Kollipara, R.; Depinho, R. A.; Gu, Y.; Simon, J. A.; Bedalov, A. *Cancer Res.* **2006**, *66*, 4368.

15. Trapp, J.; Jochum, A.; Meier, R.; Saunders, L.; Marshall, B.; Kunick, C.; Verdin, E.; Goekjian, P.; Sippl, W.; Jung, M. *J. Med. Chem.* **2006**, *49*, 7307.
16. Gey, C.; Kyrylenko, S.; Hennig, L.; Nguyen, L. H.; Büttner, A.; Pham, H. D.; Giannis, A. *Angew Chem., Int. Ed.* **2007**, *46*, 5219.
17. Chakrabarty, S. P.; Saikumari, Y. K.; Bopanna, M. P.; Balaram, H. *Mol. Biochem. Parasitol.* **2008**, *158*, 139.
18. Borra, M. T.; Langer, M. R.; Slama, J. T.; Denu, J. M. *Biochemistry* **2004**, *43*, 9877.
19. Smith, B. C.; Denu, J. M. *Biochemistry* **2007**, *46*, 14478.
20. Asaba, T.; Suzuki, T.; Ueda, R.; Tsumoto, H.; Nakagawa, H.; Miyata, N. *J. Am. Chem. Soc.* **2009**, *131*, 6989.
21. Schuetz, A.; Min, J.; Antoshenko, T.; Wang, C. L.; Allali-Hassani, A.; Dong, A.; Loppnau, P.; Vedadi, M.; Bochkarev, A.; Sternglanz, R.; Plotnikov, A. N. *Structure* **2007**, *15*, 377.
22. Shen, J.; Woodward, R.; Kedenburg, J. P.; Liu, X.; Chen, M.; Fang, L.; Sun, D.; Wang, P. G. *J. Med. Chem.* **2008**, *51*, 7417.
23. Chen, Y.; Lopez-Sanchez, M.; Savoy, D. N.; Billadeau, D. D.; Dow, G. S.; Kozikowski, A. P. *J. Med. Chem.* **2008**, *51*, 3437.
24. Bhat, R. G.; Sinha, S.; Chandrasekaran, S. *Chem. Commun.* **2002**, *8*, 812.
25. Sinha, S.; Ilankumaran, P.; Chandrasekaran, S. *Tetrahedron Lett.* **1999**, *40*, 771.
26. Ramesh, R.; De, K.; Gupta, S.; Chandrasekaran, S. *J. Chem. Sci.* **2008**, *120*, 163.
27. Rostovtsev, V. V.; Green, L. G.; Fokin, V. V.; Sharpless, K. B. A. *Angew. Chem., Int. Ed.* **2002**, *41*, 2596.
28. A typical application of click chemistry to make peptide-sugar conjugates can be found: Wan, Q.; Chen, J.; Chen, G.; Danishefsky, S. J. *J. Org. Chem.* **2006**, *71*, 8244.
29. Hunsen, M.; Long, D. A.; Ardenne, C. R. D.; Smith, A. L. *Carbohydr. Res.* **2005**, *340*, 2670.
30. Cottaz, S.; Brimacombe, J. S.; Ferguson, M. A. *Carbohydr. Res.* **1993**, *247*, 341.
31. Brady, T. P.; Kim, S. H.; Wen, K.; Kim, C.; Theodorakis, E. A. *Chem. Eur. J.* **2005**, *11*, 7175.
32. Segel, I. *Enzyme Kinetics Behavior and Analysis of Rapid Equilibrium and Steady-State Enzyme Systems*; John Wiley & Sons: New York, 1993. pp 465–504.
33. Cornish-Bowden, A. *Fundamentals of Enzyme Kinetics*; Portland Press: London, 1995. Chapter 5.
34. Santimone, M.; Koukiekolo, R.; Moreau, Y.; Le Berre, V.; Rougé, P.; Marchis-Mouren, G.; Desseaux, V. *Biochim. Biophys. Acta* **2004**, *1696*, 181.
35. Jackson, M. D.; Schmidt, M. T.; Oppenheimer, N. J.; Denu, J. M. *J. Biol. Chem.* **2003**, *278*, 50985.
36. Min, J.; Landry, J.; Sternglanz, R.; Xu, R. M. *Cell* **2001**, *105*, 269.
37. Sanders, B. D.; Zhao, K.; Slama, J. T.; Marmorstein, R. *Mol. Cell.* **2007**, *25*, 463.
38. Prusty, D.; Mehra, P.; Srivastava, S.; Shivange, A. V.; Gupta, A.; Roy, N.; Dhar, S. K. *FEMS Microbiol. Lett.* **2008**, *282*, 266.
39. Verotta, L.; Appendino, G.; Bombardelli, E.; Brun, R. *Bioorg. Med. Chem. Lett.* **2007**, *17*, 1544.
40. Duraisingh, M. T.; Voss, T. S.; Marty, A. J.; Duffy, M. F.; Good, R. T.; Thompson, J. K.; Freitas-Junior, L. H.; Scherf, A.; Crabb, B. S.; Cowman, A. F. *Cell* **2005**, *121*, 13.
41. Christopher, J. T.; Cé line, K. C.; Duraisingh, M. T.; Till, S. V.; Stuart, A. R.; Mirja, H.; Michael, F. D.; da Silva, L. M.; Scherf, A.; Ivens, A.; Speed, T. P.; Beeson, J. G.; Cowman, A. F. *PLoS Biol.* **2009**, *7*, e1000084.
42. Laemmli, U. K. *Nature* **1970**, *227*, 680.
43. Bradford, M. M. *Anal. Biochem.* **1976**, *72*, 248.
44. Trager, W.; Jensen, J. B. *Science* **1976**, *193*, 673.
45. Desjardins, R. E.; Canfield, C. J.; Haynes, J. D.; Chulay, J. D. *Antimicrob. Agents Chemother.* **1979**, *16*, 710.